ChemPubSoc Europe

DOI: 10.1002/cplu.201402137

Tin Nanoparticles in Carbon/Silica Hybrid Materials by the Use of Twin Polymerization

Christian Leonhardt,[a] Susann Brumm,[a] Andreas Seifert,[b] Arno Lange,[c] Szilard Csihony,[c] and Michael Mehring*[a]

In memory of Gerhard Cox

Simultaneous twin polymerization was used to synthesize hybrid materials composed of tin oxide, silica, and a phenolic resin starting from a mixture of 2,2′-spirobi[4*H*-1,3,2-benzodioxasiline] (Si-spiro) with either the tin(IV) alkoxides 2,2′-spirobi[4*H*-1,3,2-benzodioxastannine] (**A**), 2,2′-spirobi[6-methyl-4*H*-1,3,2-benzodioxastannine] (**B**), and 2,2′-spirobi[6-methoxy-4*H*-1,3,2-benzodioxastannine] (**C**) or the novel tin(II) alkoxides tin(II)-2-(oxidomethyl)-4-methoxyphenolate (**D**) and tin(II)-2-(oxidomethyl)-5-methoxyphenolate (**E**). In addition, the twin polymerization of the twin monomer Si-spiro in the presence of tin-containing additives, such as $Sn(OtBu)_4$, $Sn(OnBu)_2$, $Sn(OAc)_4$, and $Sn(OAc)_2$, was investigated for comparison. The as-prepared hybrid materials were characterized using solid-state NMR spectroscopy (^{13}C, ^{29}Si, ^{119}Sn) and high-angle annular dark field scanning transmission electron microscopy, and were finally converted under Ar/H_2 atmosphere at 600 °C to tin nanoparticles (10–200 nm) in porous carbon/silica hybrid materials ($Sn/C/SiO_2$) with BET surface areas up to 352 $m^2 g^{-1}$.

Introduction

The interest in nanostructured hybrid materials composed of homogeneously dispersed tin nanoparticles in a SiO_2 matrix has grown rapidly in recent years. This is attributed to potential applications in various fields such as semiconductors,[1–3] optoelectronics,[4–6] photovoltaics,[7] and anode materials for Li-ion batteries.[8,9] For example, Hwang et al. reported recently the one-pot synthesis of tin embedded in carbon/silica hybrid materials starting from organotin compounds and demonstrated the performance of such composites as anode materials for lithium-ion batteries.[10] This represents an interesting approach with regard to size control and homogeneous distribution of the embedded tin nanoparticles within the silica matrix. However, organotin compounds such as those used in the study (tributylphenyltin or tributylstannane) should be avoided in future industrial applications because of their toxic nature.[11,12] Herein, a novel approach based on less toxic tin alkoxides and carboxylates is presented. Previously, the preparation of hybrid materials composed of tin oxide, silica, and a phenolic resin by the use of the simultaneous twin polymerization route starting from novel tin(IV) alkoxides was reported.[13] The special character of this type of twin polymerization is the formation of three different materials in a coupled reaction sequence starting from two molecular precursors, here denoted as twin monomers.[14–20] The different materials are cross-linked in the hybrid material, which prevents phase separation and leads to bicontinuous networks with domain sizes of a few nanometers. Herein, an extension of this approach to prepare tin embedded in carbon/silica hybrid materials under reducing conditions is presented (Scheme 1).

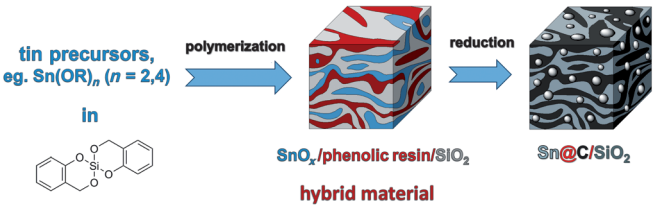

Scheme 1. Novel approach for tin embedded in carbon/silica hybrid materials based on twin polymerization.

In this process the SiO_2 acts as a crystal growth inhibitor and prevents sintering of the tin nanoparticles even at temperatures well above the melting point of tin. Thus, uniformly distributed tin nanoparticles in a carbon/silica matrix are made accessible. In addition to the previously reported tin(IV) alkoxides,[13] tin(II) alkoxides as well as nonpolymerizable tin precursors (alkoxides and acetates) were probed as additives in the twin polymerization process.

[a] *C. Leonhardt, S. Brumm, Prof. Dr. M. Mehring*
Institut für Chemie, Professur Koordinationschemie
Fakultät für Naturwissenschaften, Technische Universität Chemnitz
Strasse der Nationen 62, 09107 Chemnitz (Germany)
Fax: (+49) (0)-371-531-21219
E-mail: michael.mehring@chemie.tu-chemnitz.de

[b] *Dr. A. Seifert*
Institut für Chemie, Professur Polymerchemie
Fakultät für Naturwissenschaften, Technische Universität Chemnitz
Strasse der Nationen 62, 09107 Chemnitz (Germany)

[c] *Dr. A. Lange, Dr. S. Csihony*
BASF SE
Carl-Bosch Strasse 38, 67056 Ludwigshafen (Germany)

Supporting information for this article is available on the WWW under http://dx.doi.org/10.1002/cplu.201402137.

Results and Discussion

Hybrid materials prepared by the use of simultaneous twin polymerization

The tin(IV) alkoxides **A**–**C** were synthesized and polymerized with the spirocyclic silicon monomer 2,2′-spirobi[4*H*-1,3,2-benzodioxasiline] (Si-spiro) in the melt to give the amorphous hybrid materials **1**–**3** composed of tin oxide, silica, and a phenolic resin according to a previously reported procedure (Figure S1 in the Supporting Information).[13] In addition, we have synthesized the novel tin(II) alkoxides **D** and **E** to probe their potential for the simultaneous twin polymerization process (Scheme 2). The reduced number of organic ligands in the tin(II) precursors as compared to the tin(IV) alkoxides decreases the carbon content in the as-prepared hybrid materials and thus the tin content should increase in the final material. Simultaneous twin polymerization of the tin(II) precursors **D** and **E** together with Si-spiro either in the melt or in solution gave the corresponding hybrid materials **4** and **5**. Solid-state ^{13}C NMR spectra show the expected signals, which are assigned to the phenolic resin with *ortho*/*ortho*′ and *ortho*/*para*′ substitution (Figure S2).[21] An additional broad ^{13}C NMR signal at about $\delta = 70$ ppm and the ^{29}Si NMR spectra with signals in the range $\delta = 92$–105 ppm are indicative of some incompletely reacted silicon precursors and/or incompletely condensed silica moieties (Figure S3). Similar observations were made previously for the twin polymerization of several derivatives of Si-spiro.[22]

The hybrid materials **4** and **5** both show the typical morphology of twin polymers with 1–2 nm sized domains as demonstrated by the high-angle annular dark field scanning transmission electron microscopy (HAADF-STEM) images (Figure 1).[14,15,17] The twin polymerization with the tin(II) alkoxide **D** in the melt results in homogeneously distributed domains within the hybrid material **4** in contrast to **5**, which was obtained from **E**. In addition twin polymerization of **D** was also performed in toluene solution to give **4s**. Treatment of the hybrid materials **1**–**4** and **4s** in an Ar/H_2 (95/5%) atmosphere at 600 °C gave **1-red**–**4-red** and **4s-red** (Scheme 2). The Brunauer–Emmett–Teller (BET) surface areas of the reduced hybrid materials **1-red** and **2-red** amount to 161 and 263 $m^2 g^{-1}$, respectively, whereas the BET surface area of **3-red** is quite low and amounts to 39 $m^2 g^{-1}$.

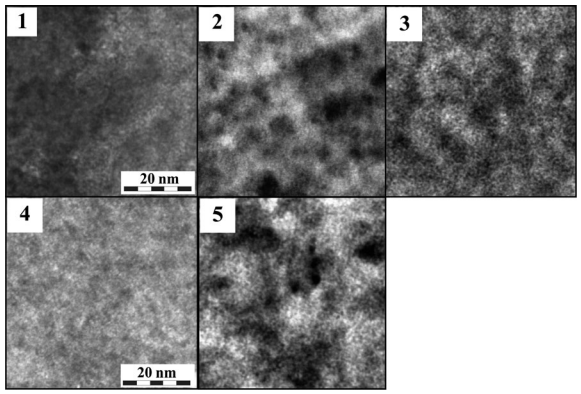

Figure 1. HAADF-STEM images of the hybrid materials **1**–**5** prepared by simultaneous twin polymerization starting from precursors **A**–**E**. (Scale bars valid for all images.)

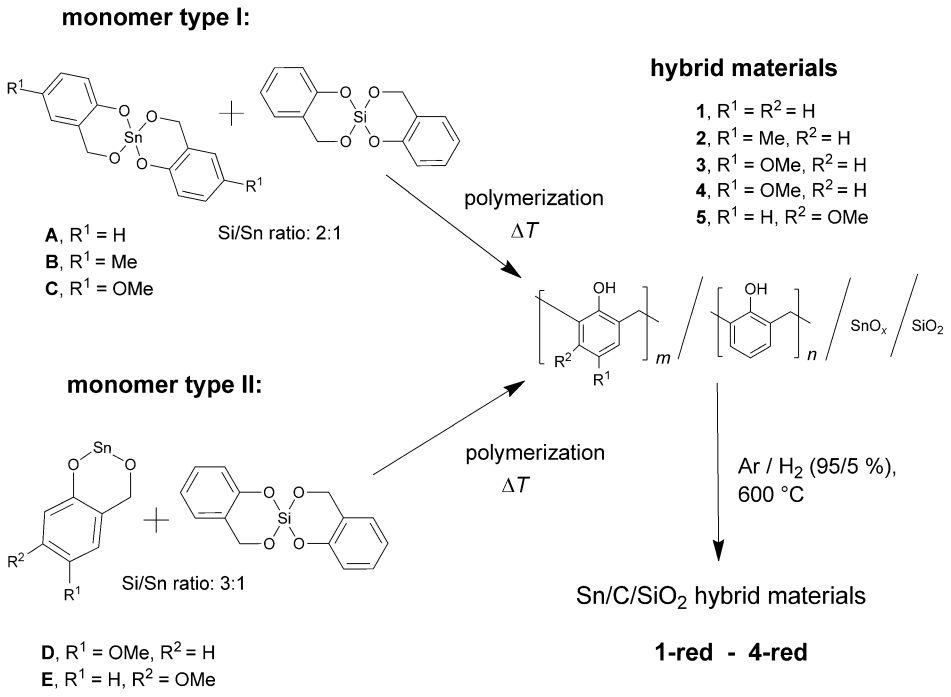

Scheme 2. Simultaneous twin polymerization of tin(II) and tin(IV) alkoxides and treatment under reducing conditions. Twin polymerization for **1**–**5** was performed in the melt.

The formation of metallic tin nanoparticles was confirmed by electron diffraction (ED) studies and X-ray powder diffraction (XRPD) analyses. Average crystallite sizes of 38 (**1-red**), 28 (**2-red**), and 40 nm (**3-red**) were calculated using the Scherrer equation (Table 1; Figure S4). The XRPD analyses are in accordance with the TEM images, which additionally provide information on the distribution of the nanoparticles within the matrix. In **1-red** the distribution of tin nanoparticles (size 15–52 nm) is homogeneous over large areas (Figure 2).

Equally sized and homogeneously distributed tin nanoparticles (13–30 nm) were determined for **2-red** (Figure 2). Compound **3-red** shows a quite homogeneous tin distribution, however, with large areas of densely and less densely packed

Table 1. BET surface areas and particle sizes of the reduced hybrid materials **1 red**–**11 red**.

Reduced hybrid materials	BET surface area [$m^2 g^{-1}$]	Average particle size [nm][a]	Tin content [wt%][b]	Carbon content [wt%][c]
1-red	161	38	29	50
2-red	263	28	n.d.	n.d.
3-red	39	40	n.d.	n.d.
4-red	78	n.d.	32	51
4 s-red	352	48	n.d.	n.d.
6-red	103	53	32	38
6 s-red	206	50	n.d.	n.d.
7-red	92	61	37	41
8-red	67	65	40	37
9-red	332	49	31	41
10-red	316	35	31	42
11-red	274	43	33	48

[a] Calculated by the Scherrer equation. [b] Measured with X-ray fluorescence analysis. [c] Measured by C,H analysis. n.d. = not determined, s = in solution.

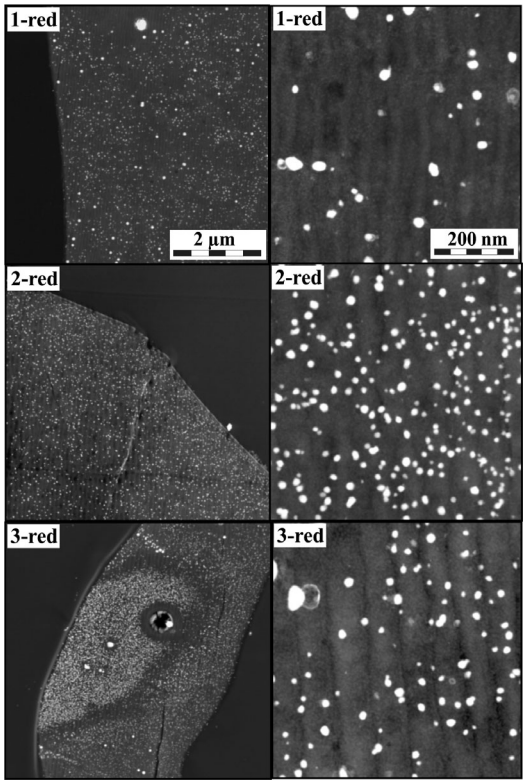

Figure 2. HAADF-STEM images of reduced hybrid materials **1-red**–**3-red**. (Scale bar valid for all images in one column.)

tin particles with sizes around 14–54 nm. In addition a few particles with sizes above 100 nm are observed. In the case of the hybrid material **4-red**, which was prepared from the novel tin(II) alkoxide **D**, homogeneously distributed tin nanoparticles with crystallite sizes from 10 to 70 nm as determined by TEM and some residual SnO_2 as determined by ED and XRPD are observed (Figure 3; Figure S5). The SnO_2 most likely results from the disproportionation[23] of tin(II) oxide at temperatures

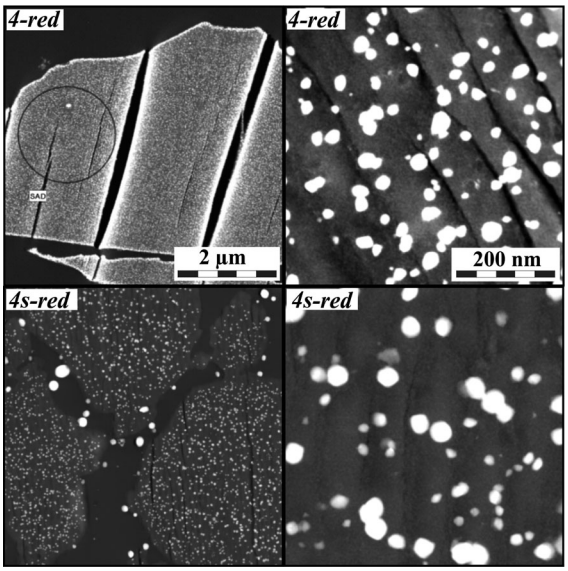

Figure 3. HAADF-STEM images of the Sn/C/SiO_2 composite materials **4-red** and **4 s-red**. (Scale bar valid for all images in one column.)

above 350 °C to give tin and tin(IV) oxide and is not completely reduced under the conditions used.

In addition a small number of tin nanoparticles are located at the interface of the hybrid material (**4-red**), which is indicative of partial phase separation (Figure 3). In contrast to materials obtained in a melt-based process (**4-red**), a larger number of tin particles are located outside the C/SiO_2 matrix for **4 s-red**, which is obtained from a solution-based process. Formation of large tin particles outside the C/SiO_2 matrix is not unexpected given 1) the temperature of 600 °C used for the reduction process (m.p. of tin 232 °C) and 2) the porous nature of the material. For example, the solution-based route for hybrid material **4 s-red** gave a surface area of 352 $m^2 g^{-1}$ after reduction. Compared to this the material produced by the melt-based process gave a BET surface area of 78 $m^2 g^{-1}$ (**4-red**). Consequently, this leads to a greater amount of leaching of tin nanoparticles to the surface for **4 s-red** than for **4-red**. However, the leaching process occurs predominantly for nanoparticles that are located close to the surface. For the hybrid material **4-red**, the TEM images reveal that leaching of tin particles from the polymer matrix can almost be neglected (Figure 3). In addition, the tin nanoparticles entrapped more deeply in the matrix do not sinter. It can be concluded that the polymerization in melt as compared with the polymerization in solution results in hybrid materials with a more densely packed polymer/SiO_2 matrix, and thus the tin nanoparticles are fixed in the following reduction process and therefore leaching is prevented.

Hybrid materials prepared by addition of tin additives

To investigate whether it is necessary to use polymerizable tin precursors such as **A**–**E** to produce homogeneously distributed tin nanoparticles by the twin polymerization process, the reaction of Si-spiro with $Sn(OtBu)_4$, $Sn(OnBu)_2$, $Sn(OAc)_4$, and

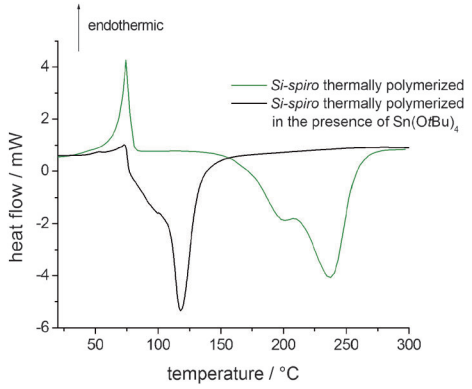

Figure 4. Differential scanning calorimetry (DSC) curve of Si-spiro thermally polymerized as compared to the polymerization of Si-spiro initiated by Sn(O*t*Bu)$_4$.

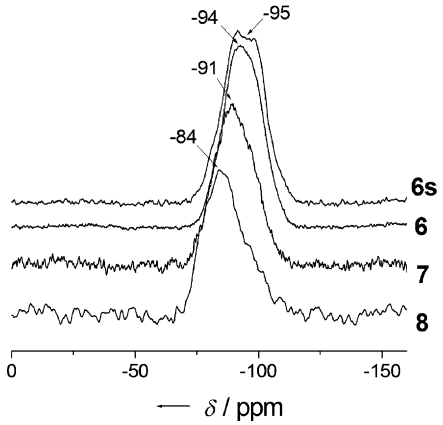

Figure 5. Solid-state ^{29}Si{^{1}H} cross-polarization magic angle spinning (CP-MAS) NMR spectra of the hybrid materials **6**–**8** and **6 s**.

Sn(OAc)$_2$ under various conditions was performed. The polymerization of Si-spiro is initiated by the Lewis acidic nature of the tin additive (Figure 4).

At first several Si/Sn ratios (2:1, **6**; 1:1, **7**; 1:2, **8**) were used for mixtures of Sn(O*t*Bu)$_4$ and Si-spiro. The polymerization reactions were performed in melt at 100 °C for half an hour and compact yellow solids were observed. For comparison, the precipitation polymerization method in toluene was used for Sn(O*t*Bu)$_4$ with a Si/Sn ratio of 2:1 to give **6 s** (Scheme 3).

Solid-state ^{13}C NMR spectra of the hybrid materials **6**–**8** show signals that are assigned to the phenolic resin with *ortho*/*ortho*′ and *ortho*/*para*′ substitution (Figure S6).[21] All samples that were polymerized in melt show, in contrast to **6 s** (precipitation polymerization method), a signal with a small width at half height at $\delta = 30$ ppm, which is indicative of *tert*-butyl groups from embedded tin species Sn(OR)$_{4-x}$(O*t*Bu)$_x$·*n* *t*BuOH (R = H, OAr) or residual *t*BuOH in the polymer. A small quantity of incompletely reacted silicon precursors and/or incompletely condensed silica is indicated by broad signals at about $\delta =$ 68 ppm in the ^{13}C NMR spectra and in the solid-state ^{29}Si NMR spectra by signals at $\delta = -95$ to -84 ppm for the hybrid materials **6**–**8** (Figure 5). Notably, the increase of the tin content leads to a shift in the ^{29}Si NMR spectra of the hybrid materials from -94 ppm (**6**) to -84 ppm (**8**), which indicates a decrease of the degree of cross-linking in the silica network.

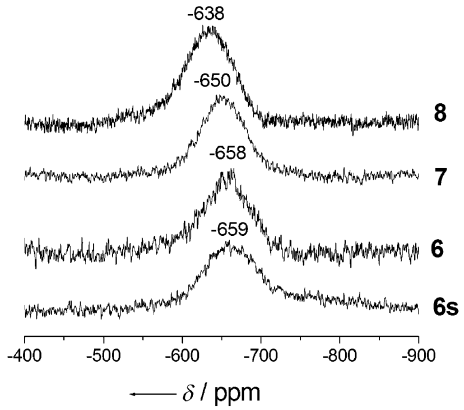

Figure 6. Solid-state ^{119}Sn{^{1}H} MAS NMR spectra of hybrid materials **6**–**8** and **6 s**.

The solid-state ^{119}Sn NMR spectra show broad signals at $\delta =$ -638 (**8**), -659 (**6 s**), -658 (**6**), and -650 ppm (**7**), which points to an incorporation of hexacoordinated tin species Sn(OR)$_{4-x}$(O*t*Bu)$_x$·*n* *t*BuOH (R = H, OAr) in the polymer matrix (Figure 6).[24–26] This assumption is reinforced by comparison of the solid-state ^{119}Sn NMR data of the tetracoordinated tin atom in Sn(O*t*Bu)$_4$ ($\delta = -371$ ppm) with the hexacoordinated tin atom in [Sn(O*i*Pr)$_4$·HO*i*Pr]$_2$ ($\delta =$ -648 ppm).[24]

HAADF-STEM analyses of the hybrid materials **6**–**8** show the typical morphology of twin polymers with 2 nm sized domains (Figure 7).[14–16] In addition to Sn(O*t*Bu)$_4$ the tin additives Sn(O*n*Bu)$_2$ and the tin carboxylates Sn(OAc)$_2$ and Sn(OAc)$_4$ were tested for their potential in the synthesis of Sn/C/SiO$_2$ materials (Scheme 3). They were mixed with Si-spiro in a Si/Sn ratio of 2:1 and polymerized in 2,6-diiso-

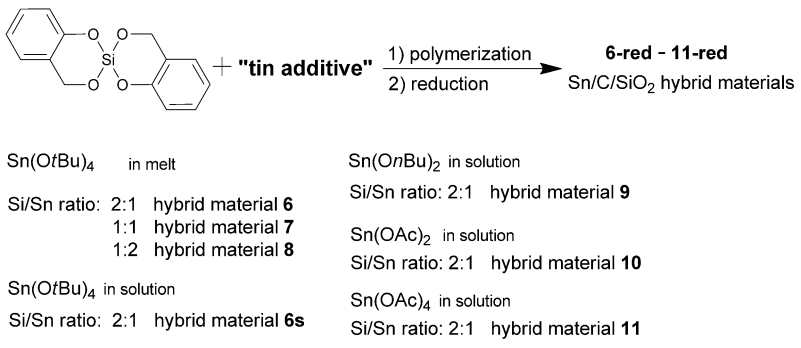

Scheme 3. 1) Polymerization of 2,2′-spirobi[4*H*-1,3,2-benzodioxasiline] in the presence of several tin additives to form SnO$_x$/polymer/SiO$_2$ hybrid materials **6**–**11**. 2) Formation of Sn/C/SiO$_2$ composites **6-red**–**11-red** by treatment of the as-prepared hybrid materials in an Ar/H$_2$ (95/5 %) atmosphere at 600 °C.

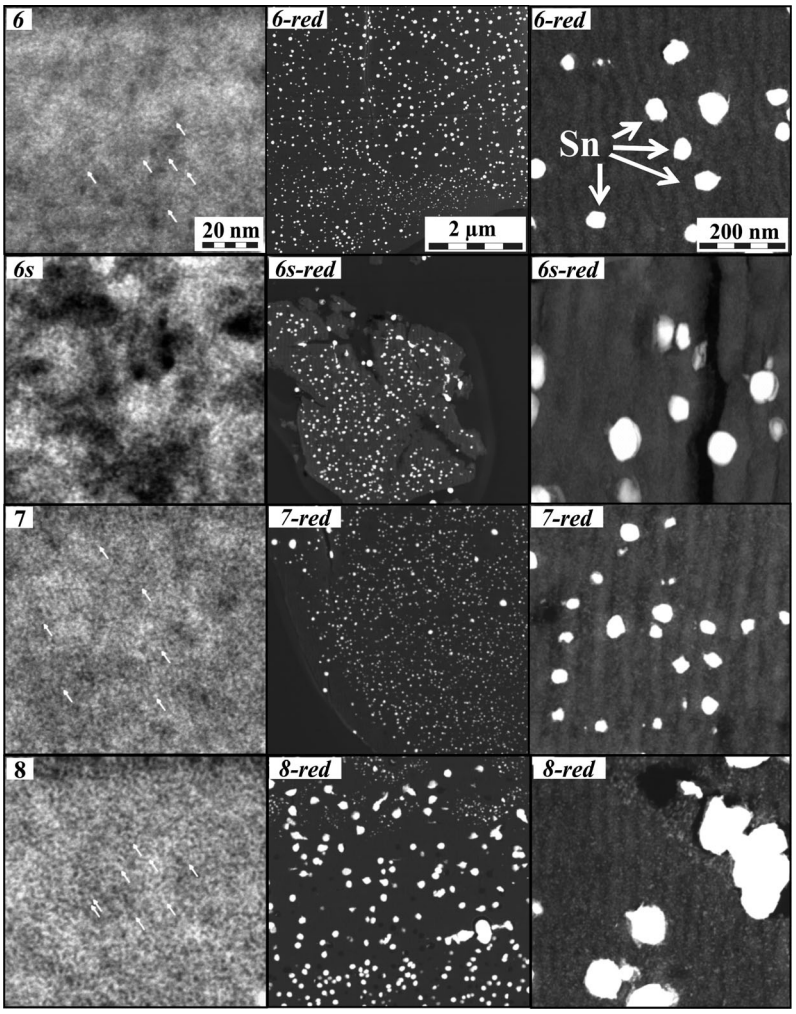

Figure 7. HAADF-STEM images of hybrid materials **6**, **6s**, **7**, and **8** (left column) and of the corresponding Sn/C/SiO_2 materials **6-red**, **6s-red**, **7-red**, and **8-red** (middle and right columns). (Scale bar valid for all images in one column.)

propylnaphthalene (for **9**) or toluene (for **10** and **11**) at 130 and 105 °C, respectively, for three hours (Scheme 3). The solid-state ^{13}C NMR spectra of the hybrid materials **10** and **11** show signals for the phenolic resin with *ortho*/*ortho*′ and *ortho*/*para*′ substitution and some residual acetic acid ($\delta = 24$ and 175 ppm, Figure S8). The solid-state ^{29}Si NMR spectra show signals at −97 (**11**) and −98 ppm (**10**), which are in the same range as those observed for the hybrid materials **6**–**8** and is indicative of incompletely condensed silica (Figure S9). After the reduction process in an Ar/H_2 atmosphere at 600 °C, the as-prepared materials **6**–**8** gave black Sn/C/SiO_2 hybrid materials with BET surface areas of 103 m^2g^{-1} for **6-red**, 92 m^2g^{-1} for **7-red**, and 67 m^2g^{-1} for **8-red** (Table 1). The full conversion into embedded tin nanoparticles is indicated by XRPD and ED measurements (Figure S7). The final tin contents for selected Sn/C/SiO_2 materials were determined by X-ray fluorescence analyses to be in the range of 29 and 40 wt% (Table 1). The amount of tin was shown to depend on the number and nature of organic ligands of the tin precursors as well as on the Sn/Si ratio used. In the reduced hybrid material **6-red** (tin content: 32 wt%; Si/Sn = 2:1) the tin nanoparticles are uniformly distributed and they are about 35–80 nm in size as determined by TEM.

The average crystallite size as calculated by the Scherrer equation amounts to 53 nm. A similar and quite homogeneous distribution of tin nanoparticles is observed for **6s-red**, which was obtained by the precipitation polymerization method (Figure 7). The average crystallite size is 50 nm (based on XRPD). However, the obtained polymer matrix is not as dense as in **6-red** and tin particles outside of the C/SiO_2 matrix as result of leaching are obtained. This observation correlates to the higher surface area of **6s-red** (206 m^2g^{-1}) relative to **6-red** (103 m^2g^{-1}). For compound **7-red** a similar average tin crystallite size of 61 nm is determined based on XRPD, but TEM images reveal an increased variation in particle size (20–120 nm), which might be assigned to the higher tin content of 37 wt% (Figure 7). Further increase of the tin content to 40 wt% in **8-red** results in tin particles that build agglomerates up to 200 nm in size even within the C/SiO_2 matrix. In conclusion, the polymerization in melt using $Sn(OtBu)_4$ as additive provides for all samples (**6-red**–**8-red**) a dense polymer matrix with embedded tin particles even for a tin content of 40 wt%. For comparison, $Sn(OnBu)_2$, $Sn(OAc)_2$, and $Sn(OAc)_4$ were used in the additive-based twin polymerization to give the hybrid materials **9**–**11** by precipitation polymerization in toluene (Scheme 3). TEM images show the typical morphology of twin polymers and tin contents between 31 and 33 wt%. Analysis of the HAADF-STEM images reveals a tin nanoparticle size within the C/SiO_2 matrix of 12–30 (**9-red**), 10–20 (**10-red**), and 10–50 nm (**11-red**) (Figure 8), in all cases accompanied by some larger particles. The crystallite sizes calculated by the Scherrer equation amount to 49 (**9-red**), 35 (**10-red**), and 43 nm (**11-red**) (Table 1; Figure S10). As result of their porous polymer matrices and high BET surface areas of 332 (**9-red**), 316 (**10-red**), and 274 m^2g^{-1} (**11-red**), large tin particles with sizes above 100 nm and increased leaching are observed for all samples (Figure 8, Table 1). In contrast to the results obtained for $Sn(OtBu)_4$ as additive in the twin polymerization process, homogeneously distributed tin nanoparticles were not obtained upon use of $Sn(OnBu)_2$, $Sn(OAc)_2$, and $Sn(OAc)_4$.

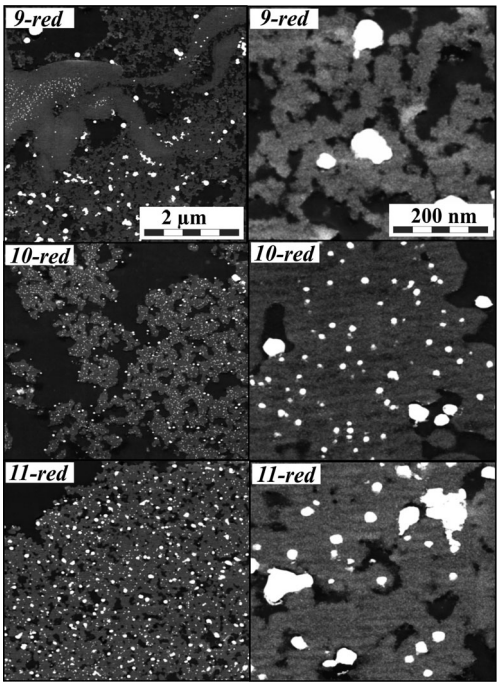

Figure 8. HAADF-STEM images of the materials **9-red**, **10-red**, and **11-red**. (Scale bar valid for all images in one column.)

Conclusion

The concept of twin polymerization was used for the synthesis of $Sn/C/SiO_2$ hybrid materials by two different approaches. The first approach was based on the simultaneous twin polymerization of 2,2′-spirobi[4*H*-1,3,2-benzodioxasiline] (Si-spiro) with tin(IV) alkoxides (**A**–**C**) and tin(II) alkoxides (**D** and **E**), which contain polymerizable organic ligands. First, hybrid materials composed of tin oxo species, silica, and a phenolic resin were observed, which after treatment under reducing conditions (Ar/H_2, at 600 °C) gave $Sn/C/SiO_2$ hybrid materials with tin nanoparticles (28–48 nm) and homogeneous distribution of the latter within the C/SiO_2 matrix. In the second approach the twin polymerization of Si-spiro was performed in the presence of different tin additives, such as $Sn(OtBu)_4$, $Sn(OnBu)_2$, $Sn(OAc)_2$, and $Sn(OAc)_4$ (additive-based twin polymerization). The polymerization was initiated by the Lewis acidic nature of the tin compounds and led successfully to hybrid materials, which were converted under reducing conditions into $Sn/C/SiO_2$ hybrid materials with tin nanoparticles embedded in the C/SiO_2 matrix. However, only $Sn(OtBu)_4$ gave a homogeneous distribution of tin nanoparticles in the matrix, similar to materials prepared by simultaneous twin polymerization. Both approaches offer the possibility to control the resulting particle size (10–200 nm) of the embedded tin particles by the use of different tin contents in the starting materials, and both processes can be performed either in the melt or in solution (precipitation twin polymerization method). However, the polymerization in melt is favored because it results in dense polymer matrices after twin polymerization, and thus leaching of tin nanoparticles and sintering during the reduction process is prevented. Materials observed by the precipitation method show high surface areas and thus increased leaching. The use of $Sn(OnBu)_2$, $Sn(OAc)_2$, and $Sn(OAc)_4$ as tin additives gave hybrid materials that showed the highest degree of leaching and a large particle size distribution, which are attributed to the porous nature of the materials with BET surface areas up to 352 $m^2 g^{-1}$. Thus, $Sn(OtBu)_4$ is favored in the additive-based twin polymerization.

Experimental Section

All reactions were performed under an inert argon atmosphere using the Schlenk technique. Chloroform was distilled over CaH_2 before use. Diethyl ether, *n*-hexane, *n*-butanol, and toluene were dried over sodium and freshly distilled prior to use. 2-(Hydroxymethyl)-4-methoxyphenol and 2-(hydroxymethyl)-5-methoxyphenol were prepared from 4-methoxyphenol and 5-methoxyphenol, respectively, using a published procedure.[27] Tin(IV) *tert*-butoxide,[24] tin(II) *n*-butoxide,[28] tin(II) acetate,[29] tin(IV) acetate,[30] tin(II) methoxide,[28] 2,2′-spirobi[4*H*-1,3,2-benzodioxasiline],[15,17] 2,2′-spirobi[4*H*-1,3,2-benzodioxastannine] (**A**),[13] 2,2′-spirobi[6-methyl-4*H*-1,3,2-benzodioxastannine] (**B**),[13] and 2,2′-spirobi[6-methoxy-4*H*-1,3,2-benzodioxastannine] (**C**)[13] were prepared according to literature procedures. Solid-state NMR measurements were performed at 9.4 T on a Bruker Avance 400 spectrometer equipped with double-tuned probes capable of magic angle spinning. $^{13}C\{^1H\}$ cross-polarization magic angle spinning (CP-MAS) NMR spectroscopy was accomplished in 4 mm rotors made of zirconium oxide spinning at 12.5 kHz. Cross-polarization with contact time of 3 ms was used to enhance sensitivity. The recycle delay was 5 s. $^{29}Si\{^1H\}$ CP-MAS NMR spectroscopy was performed in 7 mm rotors spinning at 5 kHz. The contact time was 3 ms and the recycle delay 5 s. $^{119}Sn\{^1H\}$ MAS NMR spectroscopy was performed in 4 mm rotors spinning at 12.5 kHz. The recycle delay was 10 s. All spectra were obtained under ^1H decoupling using a two-pulse phase modulation sequence. The spectra were referenced with respect to tetramethylsilane using tetrakis(trimethylsilyl)silane and tetracyclohexylstannane as standards (3.6 ppm for ^{13}C, −9.5 ppm for ^{29}Si, −97.3 ppm for ^{119}Sn). If not stated otherwise, all spectra were acquired at room temperature. X-ray powder diffraction (XRPD) analysis was performed with a STOE-STADI-P powder diffractometer with $CuK_{\alpha1}$ radiation in the range 5–70° for 2θ. Brunauer–Emmett–Teller (BET) surface area measurements were performed with a Micromeritics gadget type Gemini S. Differential scanning calorimetry (DSC) experiments were determined by using a Mettler Toledo DSC 30 instrument with a 40 µL aluminum crucible. The measurements were performed up to 350 °C with a heating rate of 10 K min^{-1} in N_2 atmosphere and a volume flow of 50 mL min^{-1}. For X-ray fluorescence analysis a MiniPal PW 4025/00 X-ray spectrometer with a rhodium anode (type TFS 5109/Rh) at 15 kV and 0.040 mA was used (regression factor = 1.6 %). HAADF-STEM analysis was performed by using an FEI Tecnai F20 field-emission TEM instrument. The samples (embedded in an epoxy resin) were ultrathin, cut by a Leica UCT ultramicrotome. The ultrathin slices were transferred onto a carbon-coated perforated copper grid.

Synthesis of tin monomers

Synthesis of tin(II)-5-methoxy-2-(oxidomethyl)-phenolate (**E**): 2-Hydroxy-4-methoxybenzyl alcohol (1.77 g, 11.5 mmol) in toluene (5 mL) was added dropwise to a suspension of tin(II) methoxide (2.08 g, 11.5 mmol) in toluene (50 mL). After stirring for 1 h at room temperature the resulting methanol was removed in vacuo and

the suspension changed to a clear solution. The remaining solvent was evaporated and the residue was washed several times with diethyl ether and dried under vacuum (10^{-3} mbar). Yield 2.78 g (10.2 mmol, 89%) of a pale yellow solid.

Decomposed at 250 °C; ^{1}H NMR (500.3 MHz, $CDCl_3$): $\delta = 6.96$ (br, 3H; aryl groups), 4.7 (br, 2H; CH_2), 3.64 ppm (br, 3H; OCH_3); $^{13}C\{^{1}H\}$ CP-MAS NMR (100.6 MHz): $\delta = 54.9$, 66.0, 103.2, 108.0, 117.8, 130.7, 157.0 159.6 ppm; $^{119}Sn\{^{1}H\}$ MAS NMR (149.2 MHz): $\delta = -422$ ppm; IR: $\tilde{\nu} = 2933$ (w), 2904 (w), 2830 (w), 1601 (m), 1570 (m), 1487 (s), 1433 (s), 1275 (s), 1194 (s), 1154 (s), 1101 (s), 1032(s), 955 (s), 829 (m), 789 (m), 733 (m), 502 (s), 443 cm^{-1} (s); elemental analysis calcd (%) for $C_8H_8O_3Sn$ (270.86): C 35.47, H 2.98; found: C 34.7, H 3.2.

Synthesis of tin(II)-4-methoxy-2-(oxidomethyl)-phenolate (**D**): The compound was prepared according to the procedure for tin(II)-5-methoxy-2-(oxidomethyl)-phenolate using $Sn(OMe)_2$ (1.23 g, 6.8 mmol), 2-hydroxy-5-methoxybenzyl alcohol (1.05 g, 6.8 mmol), and toluene (50 mL). Yield 1.50 g (5.5 mmol, 81%) of a pale yellow solid.

Decomposed at 260 °C; ^{1}H NMR (500.3 MHz, $CDCl_3$): $\delta = 6.66$ (br, 3H; aryl groups), 4.7 (br, 2H; CH_2), 3.66 ppm (br, 3H; OCH_3); $^{13}C\{^{1}H\}$ CP-MAS NMR (100.6 MHz): $\delta = 55.1$, 65.7, 111.2, 116.2, 127.9, 149.2, 153.5 ppm; $^{119}Sn\{^{1}H\}$ MAS NMR (149.2 MHz): $\delta = -420$ ppm; IR: $\tilde{\nu} =$ 2939 (w), 2901 (w), 2830 (w), 1603 (w), 1576 (w), 1479 (s), 1423 (m), 1263 (m), 1198 (s), 1150 (s), 1115 (w), 1032(s), 928 (w), 855 (m), 791 (s), 635 (m), 507 (s), 434 cm^{-1} (s); elemental analysis calcd (%) for $C_8H_8O_3Sn$ (270.86): C 35.47, H 2.98; found: C 35.0, H 3.1.

Synthesis of hybrid materials

Hybrid materials **1**–**3** were prepared from 2,2′-spirobi[4*H*-1,3,2-benzodioxastannine] (**A**; 0.70 g, 1.9 mmol), 2,2′-spirobi[6-methyl-4*H*-1,3,2-benzodioxastannine] (**B**; 0.60 g, 1.5 mmol), and 2,2′-spirobi[6-methoxy-4*H*-1,3,2-benzodioxastannine] (**C**; 0.60 g, 1.4 mmol) in combination with 2,2′-spirobi[4*H*-1,3,2-benzodioxastannine] by using a published procedure.[13]

Hybrid material **4**: 2,2′-Spirobi[4*H*-1,3,2-benzodioxasiline] (1.80 g, 6.6 mmol) and tin(II)-2-(oxidomethyl)-4-methoxyphenolate (**D**; 0.60 g, 2.2 mmol) were dissolved in chloroform (20 mL). The solvent was removed after stirring for a few minutes and the mixture was heated slowly to 90 °C for half an hour. The yellow solid was washed with acetone (15 mL) and dried at 70 °C.

Hybrid material **4s**: A precipitation polymerization method in toluene was used. 2,2′-Spirobi[4*H*-1,3,2-benzodioxasiline] (3.0 g, 11.0 mmol) and tin(II)-2-(oxidomethyl)-4-methoxyphenolate (**D**; 1.0 g, 3.7 mmol) were suspended in toluene (20 mL) and heated to 100 °C for 3 h. At 80 °C the suspension changed to a clear solution and at 95 °C a precipitate was formed. After stirring for 3 h at 100 °C the colorless solid was isolated by filtration, washed with acetone (15 mL), and dried at 70 °C.

Hybrid material **5**: 2,2′-Spirobi[4*H*-1,3,2-benzodioxasiline] (1.80 g, 6.6 mmol) and tin(II)-2-(oxidomethyl)-5-methoxyphenolate (**E**; 0.60 g, 2.2 mmol) were dissolved in chloroform (20 mL). The solvent was removed after stirring for a few minutes and the mixture was heated slowly to 90 °C for half an hour. The light red solid was washed with acetone (15 mL) and dried at 70 °C.

Hybrid materials **6**–**8**: 2,2′-Spirobi[4*H*-1,3,2-benzodioxasiline] (1.0 g, 3.7 mmol) and $Sn(OtBu)_4$ were mixed with Si/Sn ratios of 2:1 (for **6**) and 1:1 (for **7**) and subsequently heated to 100 °C for 30 min. The reaction mixture with a Si/Sn ratio of 1:2 (for **8**) was heated to 120 °C under vacuum (to remove *t*BuOH) for 1 h. The yellow solid was washed with acetone (15 mL) and dried at 70 °C.

Hybrid material **6s**: 2,2′-Spirobi[4*H*-1,3,2-benzodioxasiline] (1.0 g, 3.7 mmol) and $Sn(OtBu)_4$ (0.75 g, 1.84 mmol) were dissolved in toluene (15 mL) and heated to 90 °C for 3 h. After stirring for 3 h at 100 °C the slightly yellow solid was isolated by filtration, washed with acetone (15 mL), and dried at 70 °C.

Hybrid material **9**: 2,2′-Spirobi[4*H*-1,3,2-benzodioxasiline] (1.40 g, 5.1 mmol) and $Sn(OnBu)_2$ (0.70 g, 2.6 mmol) were suspended in 2,6-diisopropylnaphthalene (12 mL). Heating to 100 °C changed the suspension to a yellow solution and at 130 °C a yellow precipitate was observed. After further stirring for 3 h at 130 °C the solid was isolated by filtration, washed with acetone (15 mL), and dried at 70 °C.

Hybrid materials **10** and **11**: 2,2′-Spirobi[4*H*-1,3,2-benzodioxasiline] (1.40 g, 5.1 mmol) and $Sn(OAc)_2$ (0.60 g, 2.5 mmol; or **10**) or $Sn(OAc)_4$ (0.90 g, 2.5 mmol; for **11**) were dissolved in toluene (20 mL). The reaction mixture was then heated to 105 °C for 3 h. A colorless solid was isolated by filtration, washed with acetone (15 mL), and dried at 70 °C.

Reduction process

All reduction processes of the hybrid materials were performed in a tube furnace with a heating rate of 5 K min^{-1}, a final reaction temperature of 600 °C, and a reaction time of 4 h in total for materials **1-red**–**3-red** and 2 h for materials **4-red**–**11-red**. The solids were treated constantly with an Ar/H_2 (95/5%) stream of flow rate 30 L h^{-1} to give black solids composed of $Sn/C/SiO_2$ in all cases.

Acknowledgements

We are grateful to BASF SE (Ludwigshafen, Germany) and the Deutsche Forschungsgemeinschaft (FOR 1497) for financial support, Janine Fritzsch and Ute Stöß for performing C,H analyses, and Prof. S. Spange for access to differential scanning calorimetry and X-ray fluorescence spectroscopy. We are very grateful to the late Dr. Gerhard Cox (BASF SE) for supporting this work with excellent TEM analysis and dedicate this article to him.

Keywords: alkoxides · nanoparticles · organic–inorganic hybrid materials · tin · twin polymerization

[1] S. Huang, Y. Chen, H. Xiao, F. Lu, *Surf. Coat. Technol.* **2010**, *205*, 2247.
[2] Y. Lei, P. Moeck, T. Topuria, N. D. Browning, R. Ragan, K. S. Min, H. A. Atwater, *Appl. Phys. Lett.* **2003**, *82*, 4262.
[3] A. Nakajima, T. Futatsugi, H. Nakao, T. Usuki, N. Horiguchi, N. Yokoyama, *J. Appl. Phys.* **1998**, *84*, 1316.
[4] S. Huang, E.-C. Cho, G. Conibeer, M. A. Green, *Thin Solid Films* **2011**, *520*, 641.
[5] X. L. Zhao, K. F. Wang, W. F. Zhang, M. J. Huang, Y. L. Mao, *Appl. Surf. Sci.* **2010**, *256*, 6427.
[6] S. Huang, E. C. Cho, G. Conibeer, M. A. Green, D. Bellet, E. Bellet-Amalric, S. Y. Cheng, *J. Appl. Phys.* **2007**, *102*, 114304.
[7] J. M. J. Lopes, F. Kremer, P. F. P. Fichtner, F. C. Zawislak, *Nucl. Instrum. Methods Phys. Res. Sect. B* **2006**, *242*, 157.
[8] H. Huang, E. M. Kelder, L. Chen, J. Schoonman, *J. Power Sources* **1999**, *81*, 362.
[9] B. Liu, A. Abouimrane, D. E. Brown, X. Zhang, Y. Ren, Z. Z. Fang, K. Amine, *J. Mater. Chem. A* **2013**, *1*, 4376.

[10] J. Hwang, S. H. Woo, J. Shim, C. Jo, K. T. Lee, J. Lee, *ACS Nano* **2013**, *7*, 1036.
[11] M. Hoch, *Appl. Geochem.* **2001**, *16*, 719.
[12] P. V. Silva, A. R. R. Silva, S. Mendo, S. Loureiro, *Sci. Total Environ.* **2014**, *466 – 467*, 1037.
[13] C. Leonhardt, S. Brumm, A. Seifert, G. Cox, A. Lange, T. Rüffer, D. Schaarschmidt, H. Lang, N. Jöhrmann, M. Hietschold, F. Simon, M. Mehring, *ChemPlusChem* **2013**, *78*, 1400.
[14] S. Grund, P. Kempe, G. Baumann, A. Seifert, S. Spange, *Angew. Chem.* **2007**, *119*, 636; *Angew. Chem. Int. Ed.* **2007**, *46*, 628.
[15] S. Spange, P. Kempe, A. Seifert, A. A. Auer, P. Ecorchard, H. Lang, M. Falke, M. Hietschold, A. Pohlers, W. Hoyer, G. Cox, E. Kockrick, S. Kaskel, *Angew. Chem.* **2009**, *121*, 8403; *Angew. Chem. Int. Ed.* **2009**, *48*, 8254.
[16] S. Spange, S. Grund, *Adv. Mater.* **2009**, *21*, 2111.
[17] F. Böttger-Hiller, R. Lungwitz, A. Seifert, M. Hietschold, M. Schlesinger, M. Mehring, S. Spange, *Angew. Chem.* **2009**, *121*, 9039; *Angew. Chem. Int. Ed.* **2009**, *48*, 8878.
[18] A. A. Auer, A. Richter, A. V. Berezkin, D. V. Guseva, S. Spange, *Macromol. Theory Simul.* **2012**, *21*, 615.
[19] T. Löschner, A. Mehner, S. Grund, A. Seifert, A. Pohlers, A. Lange, G. Cox, H.-J. Hähnle, S. Spange, *Angew. Chem.* **2012**, *124*, 3312; *Angew. Chem. Int. Ed.* **2012**, *51*, 3258.
[20] P. Kitschke, A. A. Auer, A. Seifert, T. Rüffer, H. Lang, M. Mehring, *Inorg. Chim. Acta* **2014**, *409 (B)*, 472.
[21] R. L. Bryson, G. R. Hatfield, T. A. Early, A. R. Palmer, G. E. Maciel, *Macromolecules* **1983**, *16*, 1669.
[22] P. Kitschke, A. A. Auer, T. Löschner, A. Seifert, S. Spange, T. Rüffer, H. Lang, M. Mehring, *ChemPlusChem* **2014**, *79*, DOI: 10.1002/cplu.201402029.
[23] D. Aurbach, A. Nimberger, B. Markovsky, E. Levi, E. Sominski, A. Gedanken, *Chem. Mater.* **2002**, *14*, 4155.
[24] M. J. Hampden-Smith, T. A. Wark, *Can. J. Chem.* **1991**, *69*, 121.
[25] J. Caruso, M. J. Hampden-Smith, A. L. Rheingold, G. Yap, *J. Chem. Soc. Chem. Commun.* **1995**, 157.
[26] N. Kishor Mal, V. Ramaswamy, S. Ganapathy, A. V. Ramaswamy, *Appl. Catal. A: Gen.* **1995**, *125*, 233.
[27] Ø. W. Akselsen, L. Skattebøl, T. V. Hansen, *Tetrahedron Lett.* **2009**, *50*, 6339.
[28] R. Gsell, M. Zeldin, *J. Inorg. Nucl. Chem.* **1975**, *37*, 1133.
[29] J. D. Donaldson, W. Moser, W. B. Simpson, *J. Chem. Soc.* **1964**, 5942.
[30] A. K. Sawyer, C. Frey, R. A. Collupy, R. I. Chase, *Syn. React. Inorg. Met.* **1989**, *19*, 969.

Received: May 6, 2014
Published online on July 10, 2014